



HAL
open science

Thermochromic LaCoO₃ selective layer for self-regulated thermal solar collectors

Daria Kharkhan, Aurélien Didelot, David Pilloud, Stéphanie Bruyère, Denis Mangin, Sylvie Migot, Silvère Barrat, Zil Fernández-Gutiérrez, Nicolas Portha, Fabien Capon

► To cite this version:

Daria Kharkhan, Aurélien Didelot, David Pilloud, Stéphanie Bruyère, Denis Mangin, et al.. Thermochromic LaCoO₃ selective layer for self-regulated thermal solar collectors. *Solar Energy Materials and Solar Cells*, 2022, 240, pp.111690. 10.1016/j.solmat.2022.111690 . hal-03936215

HAL Id: hal-03936215

<https://hal.univ-lorraine.fr/hal-03936215v1>

Submitted on 22 Jul 2024

HAL is a multi-disciplinary open access archive for the deposit and dissemination of scientific research documents, whether they are published or not. The documents may come from teaching and research institutions in France or abroad, or from public or private research centers.

L'archive ouverte pluridisciplinaire **HAL**, est destinée au dépôt et à la diffusion de documents scientifiques de niveau recherche, publiés ou non, émanant des établissements d'enseignement et de recherche français ou étrangers, des laboratoires publics ou privés.



Distributed under a Creative Commons Attribution - NonCommercial 4.0 International License

Thermochromic LaCoO₃ selective layer for self-regulated thermal solar collectors

Daria N. Kharkhan^{a,b}, Aurélien Didelot^a, David Pilloud^a, Stéphanie Bruyère^a, Denis Mangin^a, Sylvie Migot^a, Silvère Barrat^a, Zil Fernández-Gutiérrez^a, Nicolas Portha^b, Fabien Capon^{a*}

^a Université de Lorraine, CNRS, IJL, F-54000 Nancy, France

^b Viessmann Faulquemont SAS, avenue André Gouy, 57380, Faulquemont, France

Abstract

Thermochromic rare-earth perovskite LaCoO₃ is a promising functional material for the new generation of selective layers and for passive regulation in thermal solar collectors. Indeed, under stagnation conditions, the solar collector overheat and this inconvenience can be skirt using a selective layer with tunable emissivity. Materials capable of reversibly switching their infrared emissivity (ϵ) at a certain temperature efficiently avoid overheating in such systems. For LaCoO₃, a distinguishable thermochromic effect is noticed starting at 77 °C. However, due to structural and chemical complexity, its design is challenging and requires a deep understanding of crystallization mechanisms. In this work, we investigate the influence of the co-deposition process of La and Co metallic targets on perovskite crystallization and optical properties of the material. All films were deposited on aluminum substrates by magnetron sputtering in the elemental or the compound mode (Ar or Ar/O₂ atmosphere) using a semi-industrial reactor with back-and-forth scrolling of the substrate. The samples were post annealed in air for 2, 5, and 10 minutes at temperatures ranging between 500 and 600°C and characterized using XRD, SIMS, TEM, and infrared camera. The measurements of infrared emissivity variation show an increase of the emissivity when the temperature raises confirming the great prospects of LaCoO₃ usage for the considered application. A prototype of a solar collector equipped with LaCoO₃ deposited in the elemental mode was built in order to demonstrate the potentiality of this perovskite as a thermoregulated selective layer.

1. INTRODUCTION

Perovskite-type oxides are a group of materials that can be described with a general formula ABO₃. Such a structure allows to embed a wide variety of metallic cations and to form therefore a range of materials with various properties. Among these properties can be distinguished thermochromism [1-7] that is the aptitude of some structures to reversibly change their behavior from insulator to metallic at a specific temperature (T_{MI}) referred to as metal-insulator transition. This transition is associated with optical changes that can be exploited, among other applications, for the development of a new generation of intelligent absorber coatings for passive thermal regulation [8, 9].

The absorber coating or a selective layer is the core element of a thermal solar collector (i.e. a collector for hot water production using solar energy). Its role is to absorb solar energy and to transfer it to a heat-transport fluid that is generally a glycol-based mixture. To ensure a good performance of the system, the coating should possess both solar absorption higher than 90 % (for wavelengths in the range $0.4 < \lambda < 0.8 \mu\text{m}$) and infrared

emissivity lower than 10 % (for wavelengths in the range $6 < \lambda < 10 \mu\text{m}$). “Stagnation conditions” or “overheating” are the terms denoting a situation when the temperature inside the collector reaches high values [220 – 250 °C] in the absence of hot water demand. These temperatures produce excessive stresses on absorber mountings or within the absorber structure itself (due to thermal expansion), furthermore without regular maintenance to replace the medium, or without the use of additional and costly regulation/purge systems (drain-back for example), the solar thermal system gradually loses its efficiency, and serious damages occur in the system such as mud formation in the piping and inside the thermal exchanger. Yet, the implementation of a thermochromic material whose emissivity increases with temperature allows evacuating excessive heat thus protecting the collector.

Up to now, the material, which is currently used in thermoregulated thermal solar absorbers, is a thermochromic alloy based on vanadium dioxide VO_2 [10]. However, even if its transition temperature of 68 °C allows to avoid the overheating problem, simulations show that the optimal regulation is achieved for a TMI around 80 °C. Furthermore, the European certification standards such as Solar Keymark [11] consider the overall performance of the solar collector, which is an average of outputs measured at 25, 50 et 75 °C. Having transited at 68 °C, a VO_2 -based collector demonstrates an emissivity of approximately 42 % at 75 °C [10]. This leads to the underestimation of the overall performance and may pose significant threats for further commercialization. Consequently, the development of another material possessing optical properties similar to those of VO_2 , but for which TMI would be higher represents an optimization for the thermochromic layer. Unfortunately, using dopants such as Cr or Al, we can achieve a mere 3 °C increase of the TMI.

Given the above, and considering it is difficult to modulate the transition temperature of VO_2 , a thermochromic perovskite represents a good solution. Among possible candidates to replace vanadium dioxide we chose rare-earth cobaltites and notably LaCoO_3 known for its stability under high temperatures and oxidizing conditions. This material undergoes two successive spin-state transitions at around -175 °C (from low to intermediate-spin state) and 220 °C (from intermediate to high-spin state) [12, 13]. The latter corresponds to the metal-insulator transition and is accompanied by a progressive change in electrical and optical behavior. At first sight, this temperature seems too high for the considered application. However, in such a material the transition is not as abrupt as in VO_2 and occurs in a wider range starting at a temperature lower than 220 °C. This indicates that LaCoO_3 may be well adapted for efficient usage in thermal solar collectors.

Lanthanum cobaltite coatings can be deposited by various methods [14-16], one of the easiest and at the same time, the most efficient of which is the magnetron sputtering technique. As for many other perovskite-type oxides, the deposition of LaCoO_3 thin films can be performed in the elemental or the compound mode followed by an air annealing.

Regardless of the mode used, *ex-situ* annealing should be performed to crystallize the amorphous metastable material obtained during the deposition stage. Even though the elemental mode presents a higher deposition rate and is easier technically, it was previously shown [17] that the way the elements are distributed in as-deposited films has a deep influence on the crystallization. Indeed, in our semi-industrial reactor, the process consists of a cyclic exposure of the substrate to the plasma of, first, cobalt and second, lanthanum during the deposition. For films deposited in the elemental mode, alternate metallic layers La and Co of some nanometer thick are observed. In the compound-mode depositions, the oxygen is already present in the as-deposited film. Due to the

lower deposition rate, the cyclic exposure will lead to thinner multilayers La₂O₃/Co₂O₃, and the resulting film will exhibit a higher chemical composition homogeneity.

In this work, we investigate the role of the deposition mode on perovskite formation mechanisms and provide the measurements of the key optical characteristic, emissivity variation ($\Delta\varepsilon$), induced by the thermochromic transition. Furthermore, we present thermoregulation results for a prototype of the solar collector equipped with a LaCoO₃ selective layer, that demonstrate a high potential of this material for the considered application.

2. EXPERIMENTAL DETAILS

All films were deposited on 21.0×29.7 cm² aluminum substrates (0.3 mm thick) by co-sputtering of two pure (99.95%) metallic targets using a semi-industrial reactor with back-and-forth scrolling. The size of the substrate has two advantages. First, sample can be divided to ensure reproducibility of the results, and second, it allows us to build a prototype of a solar collector. Both metallic targets have a rectangular shape and measure 330×50 mm² each. The thickness of the lanthanum target is 6 mm, and that of the cobalt target was reduced to 2 mm in order to take advantage of the magnetic field of the magnetron cathode across the ferromagnetic target. The targets were placed at a fixed distance of 50 mm from the moving substrate and were powered by pulsed DC generators (Advanced Energy Pinnacle Plus®). The flow rates of gases were controlled in standard cubic centimeters per minute (sccm). a throttle valve, the working pressure in the chamber was maintained at 1 Pa for the compound mode and 2 Pa for the elemental mode. All films were synthesized at room temperature. Even though the substrate was not intentionally heated, it should be considered that its temperature increases progressively during the compound mode depositions. However, based on our previous observations, we can assume that the attained temperatures (lower than 80 °C) are not high enough for *in-situ* annealing and the films keep the amorphous metastable structure.

The overall stoichiometric ratio La : Co = 1 : 1 was achieved by fixing the power delivered on the La target while adjusting the power applied to the Co target. The ratios were then evaluated by the EDS analysis using a Philips FEG XL 30 scanning electron microscope (SEM).

As-deposited films were annealed in air at temperatures in the range [500-600 °C] in a Carbolite HRF 7/45 furnace. Annealings were performed every 20 °C for 2, 5 and 10 minutes. The thicknesses of the films before and after the treatment were measured using a GBS smartWLI 3D optical profiler.

The structure of the annealed films was evaluated by X-ray diffraction (XRD) using Bruker D8 Advance equipment in Bragg-Brentano configuration with CuK α 1 radiation ($\lambda = 0.15406$ nm). The results were then analyzed using the Bruker EVA software.

Depth profiles of the films were obtained by Secondary Ion Mass Spectroscopy (SIMS) performed with Cs⁺ ions using Cameca IMS7F equipment.

The optical properties vs. temperature i.e. variation of emissivity ($\Delta\varepsilon$) were calculated according to the standard ISO 22975-3:2014 (Solar energy - Collector components and materials - Part 3: Absorber surface durability) using Fourier-transform infrared spectroscopy (FTIR). The reflectance of the samples was measured for temperatures going from 30 to 300 °C for wavelengths in the range between 2500 and 25000 nm.

Wien's displacement law (Eq.1) was used to calculate the emissivity of the black body normalized at each temperature.

$$\lambda_{max} = \frac{2.898 \times 10^{-3}}{T}, \quad (\text{Eq.1})$$

where λ_{max} – the maximum wavelength (m) and T – temperature (K).

For a given temperature, the difference between the integral of the reflectance of the sample and that of the black body is equal to the absorbed radiation $\alpha(T)$, which in its turn is equal to the emissivity of the material $\varepsilon(T)$, as we consider that thermic radiation is isotropic. The emissivity variation ($\Delta\varepsilon$) between 30 and 300 °C is thus calculated as $\varepsilon(300 \text{ °C}) - \varepsilon(30 \text{ °C})$. A graphic representation of the method for an elemental-mode prepared sample used for the fabrication of the prototype is given in Fig. 1. The blue area corresponds to the emissivity $\varepsilon(T)$ at a given temperature.

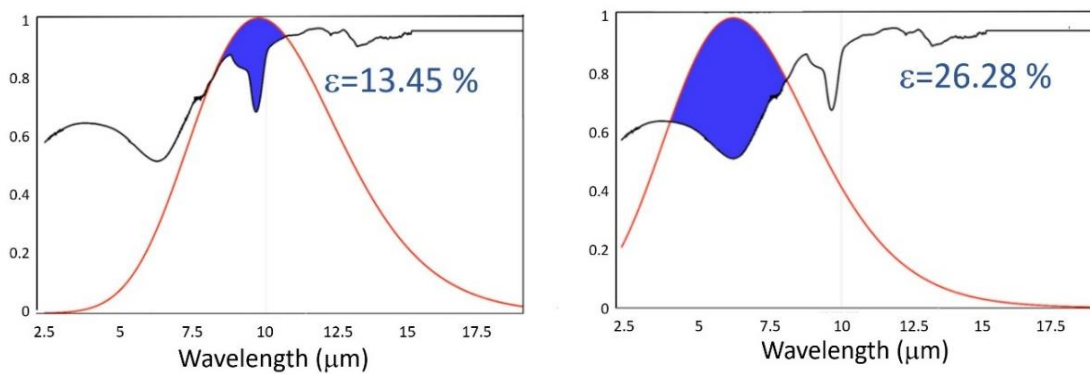


Fig. 1. Emissivity measurements for elemental mode deposited samples at
a – 30 °C, **b** – 300 °C.

Finally, the influence of pre-oxidation on the film microstructure was evaluated using a High-Resolution Transmission Electron Microscope (HR-TEM) JEOL ACCEL ARM 200-Cold FEG with a resolution of 0.12 nm in the TEM mode. The elemental composition was investigated using TEM in scanning mode (STEM) and the JEOL Centurio (1sr of active surface) detector for Energy Dispersive X-Rays Spectroscopy (EDS) analysis.

3. RESULTS AND DISCUSSIONS

3.1 Compound vs. elemental mode

As it was mentioned before, as-deposited films synthesized in the elemental mode have a pronounced multi-layer distribution of Co and La with alternating layers of pure metals of 10-12 nm each. The origin of this phenomenon is the cyclic exposure of the substrate to the plasma of the corresponding metals which in its turn is conditioned by the configuration of the reactor itself and cannot, therefore, be completely eliminated at the deposition stage.

Thus, for elemental-mode-prepared films, the perovskite is formed during the annealing treatment owing to the Kirkendall effect and the diffusion of oxygen. The Gibbs energy formations of the CoO and La₂O₃ oxides are highly negative (as we can observe on the oxide Ellingham diagram) and much more negative than the corresponding Gibbs energy of formation for the perovskite. Consequently, at the annealing temperature of 600 °C, the direct crystallization of the oxides would correspond to the formation of the most stable phases and the

inability to obtain the perovskite compound.[18] The effective crystallization of the perovskite suggests that metastable amorphous metallic layers persist during the annealing, and oxygen diffuses through them without elemental oxide crystallization. When the oxygen concentration is sufficiently high at the amorphous metallic layer interfaces Co/La, a perovskite layer could directly crystallize without the formation of the intermediate elemental oxide compounds.

Considering this, we can assume that LaCoO_3 is formed directly at the interfaces between two metals due to the interdiffusion of the atoms of cobalt, lanthanum, and oxygen, and its quantity increases as the annealing proceeds.

With the diffusion flow from an element A into an element B (Fick's first law) being: $\overline{J}_A^B = -D_A^B \overline{\text{grad}} C_A^B$ (where D_A^B is the intrinsic diffusion coefficient of the element A into the element B and C_A^B – the concentration of the element A in the element B), and given that $J_{\text{Co}}^{\text{La}} > J_{\text{La}}^{\text{Co}}$ [19], we can assume that interdiffusion only occurs if the structure contains vacancies. In this case $J_{\text{La}}^{\text{Co}} + J_{\text{Co}}^{\text{La}} + J_l = 0$.

As the crystal lattice should move in the direction of the flow of vacancies J_l at a speed $v = (D_{\text{Co}}^{\text{La}} - D_{\text{La}}^{\text{Co}}) \frac{\partial c_{\text{Co}}^{\text{La}}}{\partial x}$, [20][21] we can estimate the interdiffusion coefficient to be $D = C_{\text{Co}}^{\text{La}} D_{\text{La}}^{\text{Co}} + C_{\text{La}}^{\text{Co}} D_{\text{Co}}^{\text{La}}$. At the same time $\Delta C \approx f(t, l, D)$, with t being the time of annealing and l the thickness of the initial metallic layers.[22]

In-situ oxidation during the compound mode is most desirable way to form an almost homogeneous material already at the deposition stage. First, oxygen is incorporated directly at the deposition stage. Second, as the presence of a reactive gas decreases the deposition rate, less material is deposited at every passage in front of the targets compared to the elemental mode. Naturally, in order to obtain the same thickness, the number of *loops* (back-and-forth passages in front of both targets) should be increased.

Compared to the elemental mode depositions that only require establishing optimal electric parameters for both targets, depositions in the compound mode also require good control of oxidation conditions. Consequently, to guarantee complete oxidation during the film synthesis, it is crucial to optimize the ratio $\text{Ar}:\text{O}_2$ introduced into the reactor. The necessary quantity of oxygen was established by studying the evolution of voltage as a function of the oxygen flow rate. For each target, the optimal values of the power that should be applied to the target in order to obtain stoichiometric films (250 and 100 W for La and Co respectively) were preliminarily determined.

Fig. 2 reports the voltage response for the Co and La targets to simultaneous power application during the oxygen cycles (i.e. oxygen flow rate increases from 0 to 10 sccm with a subsequent decrease back to 0 sccm).

For the La target, the initial value of voltage corresponding to the elemental mode is about 200 V. However, due to its high reactivity, the progressive introduction of oxygen leads to an abrupt decrease for flow rates in the range between 0 and 1.5 sccm, and further stabilization for flow rates higher than 2 sccm. The passage to stable electric parameters indicates the transition from the elemental to the compound mode. [23]

For the Co target, similar behavior is observed with the difference that the voltage, the initial value of which is about 380 V, first increases with the increment of oxygen quantity (for flow rates between 0 and 2 sccm) and then starts to slightly decrease before finally stabilizing (for flow rates higher than 5 sccm).

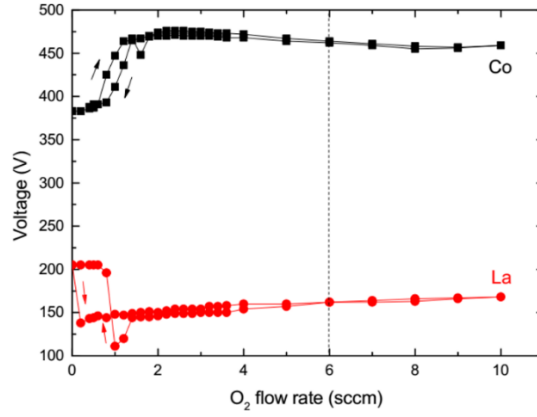


Fig. 2. Evolution of voltage as a function of oxygen flow rate for simultaneously sputtered cobalt and lanthanum targets.

For both targets, well-defined hysteresis loops caused by the getter effect can be observed for low values of oxygen flow rates. We can assume that a stable compound mode is attained for oxygen flow rates of 6 sccm and higher.

Key compound and elemental mode (first reported in [19]) deposition parameters are presented in Table I.

Table I. Main deposition parameters for elemental and compound modes

Working pressure	elemental	2 Pa
	compound	1 Pa
Ar flow rate (both modes)		50 sccm
O ₂ flow rate (compound)		6 sccm
Power on La target:	elemental	120 W
	compound	250 W
Power on Co target:	elemental	115 W
	compound	100 W

3.2 Evaluation of crystallographic structure

Compared to the elemental mode, the deposition rate of the compound mode is divided by 7. As consequence, the deposition process in the compound mode should be run for about 300 minutes instead of 42 to reach the same optimized pre-annealing thickness of 420 nm that lead to an optical performance $\Delta\epsilon = 56\%$. Unfortunately, such a duration is not compatible with requisites of any industrial process. Given that the process will have to be industrialized and in order to compare the optical performance of films prepared by different methods, we chose to grow films of 200 nm both in the elemental and compound modes. Still, regardless of the method, as-deposited films should be annealed in air in order to oxidize (elemental mode) and crystallize (both modes) the structure. These annealing were performed during 2, 5 and 10 minutes every 20 °C for temperatures in the range [500-600 °C]. The structure and the crystallinity of the films were then evaluated by X-ray diffraction. Fig. 3 shows the XRD diffractograms of the thin films annealed in the range [500-600 °C]. Thin films deposited in elemental mode crystallize after 5 minutes at the temperature of 600 °C (for a treatment of 2

minutes thin film remains amorphous). Thin films deposited in compound mode crystallize after 2 minutes at the temperature of 600 °C.

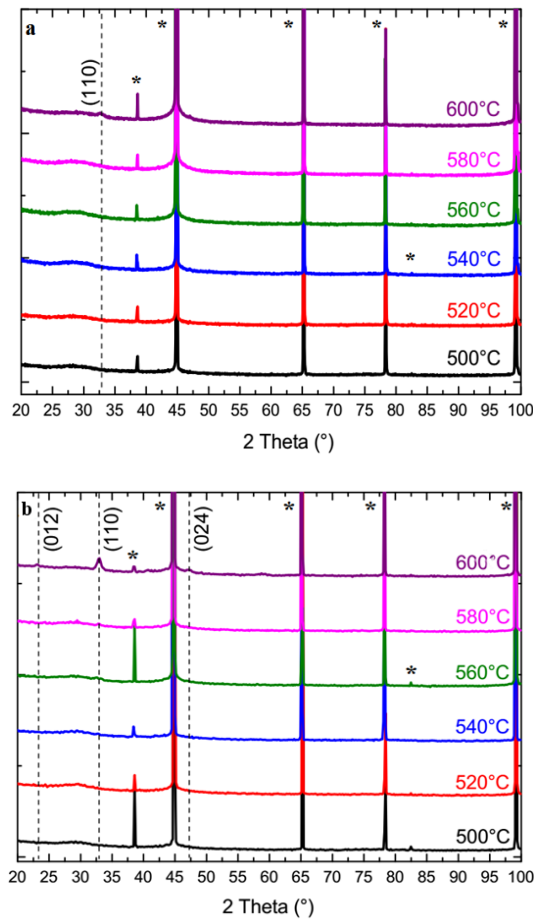


Fig. 3. Diffraction patterns for 200 nm thick LaCoO_3 films annealed in air at different temperatures for 5 minutes deposited in a – elemental mode, and for 2 minutes deposited in b – compound mode. The peaks corresponding to the aluminum substrate are marked with the symbol *.

The best results were obtained for 10 minutes treatments. Fig. 4 presents diffraction patterns for annealed films prepared in both modes of deposition. Pre-oxidized films start to form the perovskite structure at a lower temperature than it does for initially metallic films. The first peak characteristic of the rhombohedral (110) planes appears at 32.88° (JCPDS 48-0123) for 520°C in the compound mode deposited films and only at 560°C for films deposited in the elemental mode. In addition, in both cases, other characteristic peaks at 23.23° (012), 40.66° (202), 47.47° (024), and 58.94° (214) start to appear at higher temperatures.

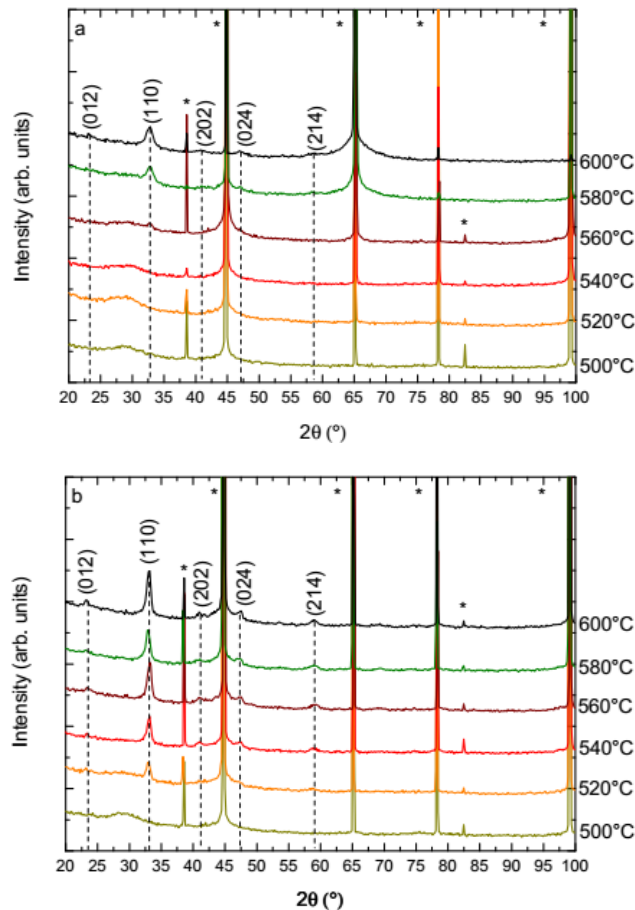


Fig. 4. Diffraction patterns for 200 nm thick LaCoO_3 films annealed in air at different temperatures for 10 minutes deposited in a – elemental mode, b – compound mode. The peaks corresponding to the aluminum substrate are marked with the symbol *.

For both modes, the peaks gradually become narrower and more intense with the temperature increment which indicates a progressive grain size increasing and more crystallinity of the material at higher temperatures. Films prepared in the compound mode exhibit grain sizes calculated with the Scherrer equation using EVA software that increase from approximately 12 to 18 nm for samples annealed respectively at 520 and 600 °C. For the films prepared in the elemental mode, the grain size of samples annealed at 560 °C is too small to be properly evaluated and is estimated to be approximately 5-8 nm. It only reaches 11 nm for samples annealed at 600 °C.

We can therefore expect that further increase of the annealing temperature will lead to the formation of a better-crystallized structure. However, considering the nature of the substrate, it is not recommended to exceed the temperature of 600 °C, at which aluminum starts to deteriorate due to the proximity of its melting point (660 °C).

For the same reason it is difficult to increase the duration of the annealing, because at 600 °C aluminum warps with the heating.

These results confirm the influence of the elaboration mode or more precisely the influence of as-deposited microstructure (i.e. elemental distribution) on the LaCoO_3 formation mechanisms.

At the same time, we can put forward a hypothesis that for the films deposited in the elemental mode, the chosen durations of the annealing are too short to ensure a complete crystallization.

3.3 Evaluation of the oxidation

SIMS analyses presented in Fig. 5 do not demonstrate any difference between a film deposited in elemental mode and annealed at 500 °C for 2 minutes and at 600 °C for 10 minutes. Particular attention should be paid to the oxygen profile (in black). Its constant signal indicates that complete oxidation takes place already for short treatments at moderate temperatures.

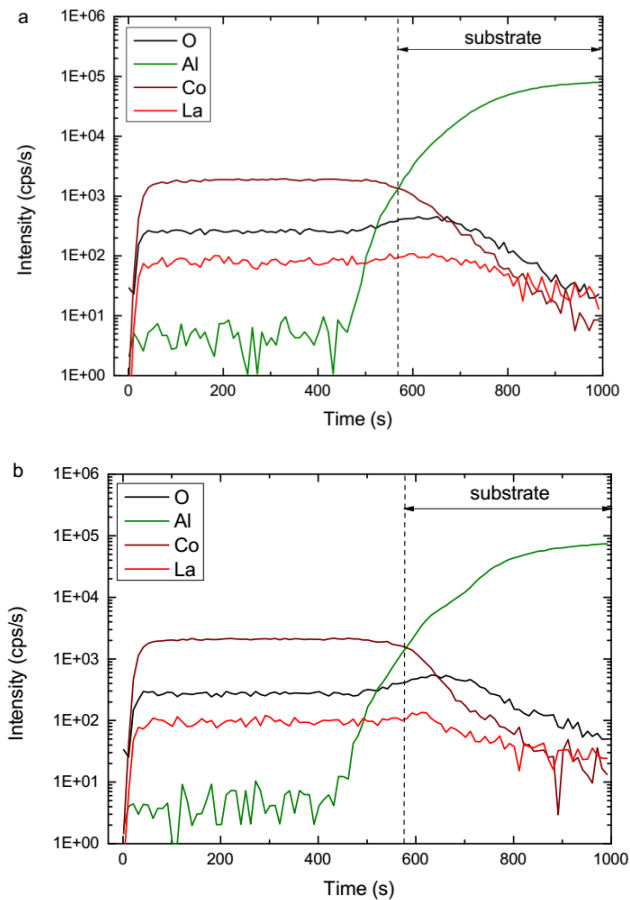


Fig. 5. SIMS depth profiles of La, Co, O and Al for a 200 nm elemental mode prepared film annealed a – at 500 °C for 2 minutes and b – at 600 °C for 10 minutes.

These results, in addition to the XRD patterns obtained (Fig. 4.a), show that the diffusion of the oxygen occurs at lower temperature than the crystallization. As consequence, the incorporation of the oxygen is not a limiting factor, and improved LaCoO_3 synthesis is attributed to the better element homogenization (thinner multilayers) in the case of as-deposited thin films growth using compound mode.

3.4 TEM microstructural characterization and evaluation of elemental distribution for compound mode prepared films

The thickness of each deposited layer that is comprised between 10 – 12 nm in the elemental mode for a scrolling speed of 100 cm/min and must be divided by 7 in the compound mode. In this mode, multilayers of La₂O₃/Co₂O₃ of about 2 nm is expected. Fig. 6 presents high angle annular dark-field (HAADF)-STEM images and a related EDS cartography for an as-deposited 200 nm thick LaCoO₃ film deposited in the compound mode. Even though the elements are still distributed in alternating layers, the thickness of these layers are difficult to distinguish even at high resolution (Fig. 5c). The material can be thus considered *quasi-homogeneous*.

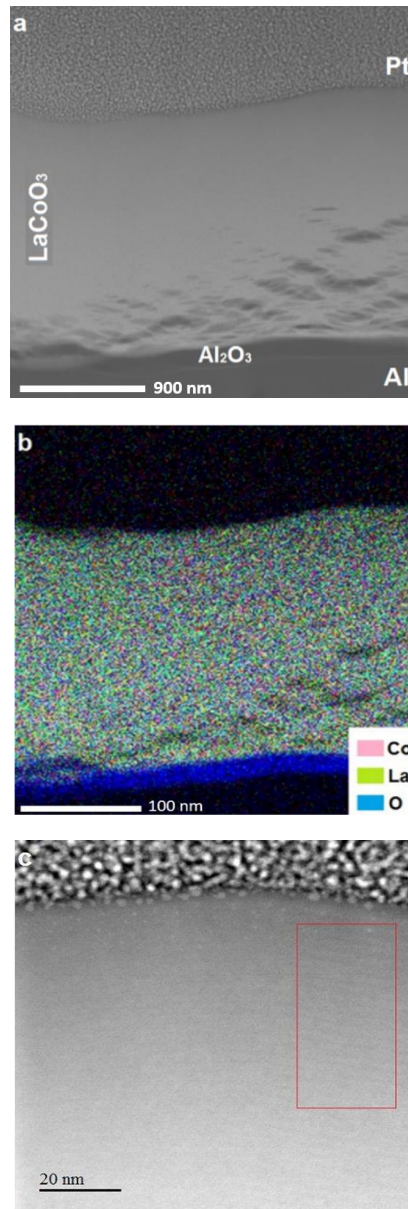


Fig. 6 HAADF-STEM image (a) with corresponding EDS cartography of 3 elements (b) and zoomed HAADF-STEM image (c) of the microstructure of an as-deposited 200 nm thick LaCoO₃ film deposited in the compound mode.

The post-annealing SAED TEM pattern presented in Fig. 7, confirms the crystallization of the LaCoO₃ perovskite even though some areas of the sample remain amorphous:

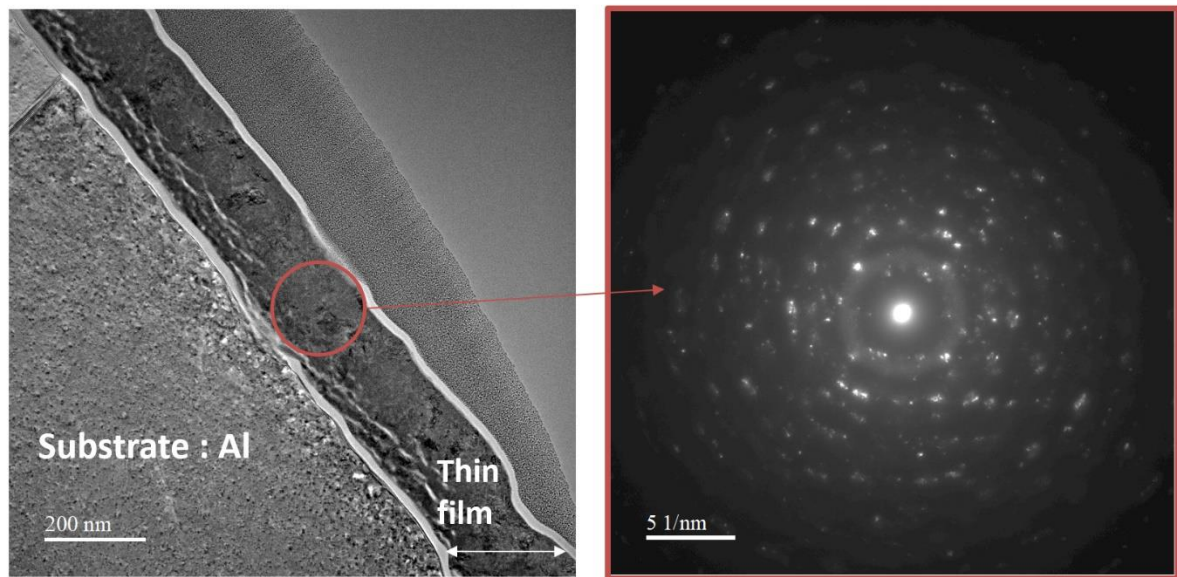


Fig. 7 TEM image of the cross-section and SAED pattern from the red area of a sample deposited in the compound mode after an air annealing at 600 °C during 10 min.

Stoichiometric homogeneity of the annealed sample was verified by STEM-EDS in Fig. 8. The thin film is homogeneous except for some areas marked with black arrows. The crystallization is associated with a solid-state diffusion which leads to a disappearance of the cobalt in some localized area of the thin film.

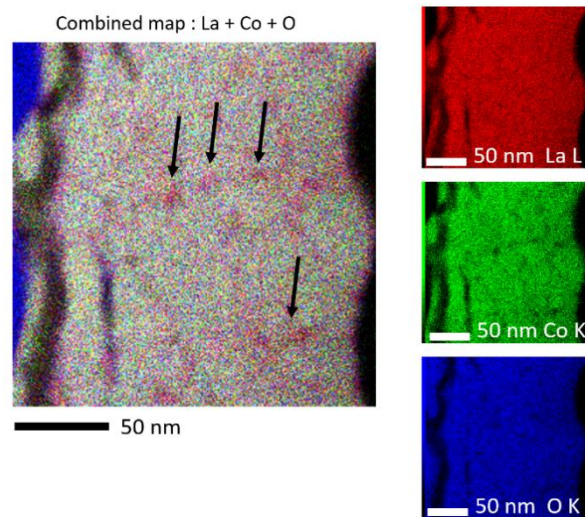


Fig. 8. STEM-EDS cartographies of thin films deposited in the compound mode after an air annealing at 600 °C during 10 minutes.

3.5 Optical characterization of films prepared in compound mode using IR camera

A series of optical characterization tests using an IR camera was performed on samples elaborated in the elemental and compound modes and annealed under different conditions. Emissivity curves obtained with the infrared camera FLIR A300 are presented for samples annealed at 600 °C for 5 and 10 minutes in Fig. 9. For

each sample, the infrared temperature is plotted against real temperature. Curves present two linear segments that appear at low and high temperatures (i.e. from either side of the TMI). The emissivity switch, $\Delta\varepsilon = \varepsilon_{HT} - \varepsilon_{LT}$ was calculated by the difference between the slopes corresponding to each region of the MIT according to the method employed by Benkahoul et al [24]. ε_{HT} is calculated in the range [350-500 °C] and ε_{LT} in the range [RT-100 °C]. For 5 minutes annealing, there is a 13% increase of $\Delta\varepsilon$ for the samples prepared in the compound mode. For the 10 minutes treatments, the difference is even more obvious with the increase of $\Delta\varepsilon$ reaching 28%.

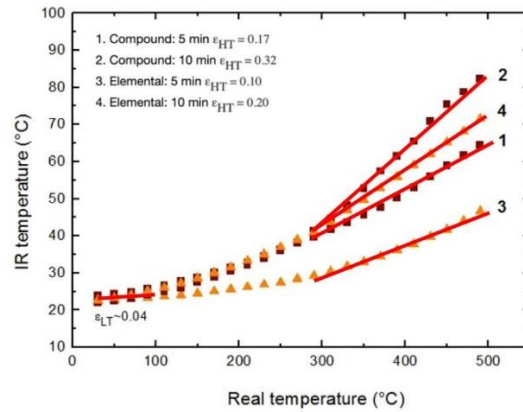


Fig. 9. Evaluation of emissivity variation for 200 nm LaCoO_3 thin films synthesized in two modes and annealed at 600 °C during 5 and 10 minutes.

Comparing $\Delta\varepsilon$ values for different samples, (table II), we can conclude that for both deposition modes there is a strong correlation between the treatment conditions and the optical behavior of the samples. Indeed, the values of emissivity variations or ε_{HT} (in accordance with the enhancement of the crystallinity previously observed by XRD) improve progressively with the temperature and duration increment.

Table II. Comparison of emissivity variation values $\Delta\varepsilon$ (%) for LaCoO_3 thin films prepared in the elemental and compound sputtering modes

Annealing temperature	Duration	Compound $\Delta\varepsilon$	Elemental $\Delta\varepsilon$
540 °C	5 min	5	n/a
	10 min	10	n/a
560 °C	5 min	7	n/a
	10 min	15	4
600 °C	5 min	13	6
	10 min	28	16

Elements homogeneity of as-deposited (La,Co,O) films synthesized in the compound mode leads to an increase of $\Delta\varepsilon$ that reach 28%. This is the best result that we manage to obtain given the industrial constraint. Although the deposition in the compound is more efficient with an $\Delta\varepsilon$ increasing from 16 to 28%, we show previously [19] that films deposited in elementary mode exhibit a variation in emissivity $\Delta\varepsilon = 56\%$. In this work, films present a thickness of 600 nm after an annealing at 600 °C during 10 min. We conclude, that in this process, the thickness is the key role to obtain the best $\Delta\varepsilon$ that excluded compound mode of the process. Indeed,

as explained in the introduction, compound deposition rate and aluminum melting point prohibit respectively the increase of the thickness, and the annealing temperature. Considering this, we decided to build a prototype using films deposited in elementary mode.

3.6 Prototype built with samples prepared in the elemental mode:

A series of 12 samples were deposited in the elemental mode by delivering the power of 120 W to the lanthanum target and the power of 115 W to the cobalt target. A total of 32 *loops* were made by the substrate at 100 cm/min, with the duration of the growth of 42 min. resulting in 420 nm thick films that would expand to 600 nm after *ex-situ* oxidation during the annealing (600 °C for 10 minutes). Note that this annealing condition are drastic for the substrate, at 600 °C aluminum warps and becomes rough.

Next, an anti-reflective SiO₂ layer of 80 nm was deposited from a silicon target in the presence of oxygen to improve solar absorption (by about 10%).

Finally, the samples were assembled into a prototype of a solar collector (Fig. 10) and tested in outdoor conditions equipped with two thermocouples (T1 and T2) attached to its rear part. T1 was located at the center of the collector and T2 at the point where the coolant flows out of the collector. In the meantime, solar irradiance was measured by a wattmeter behind the collector operating in the visible range.

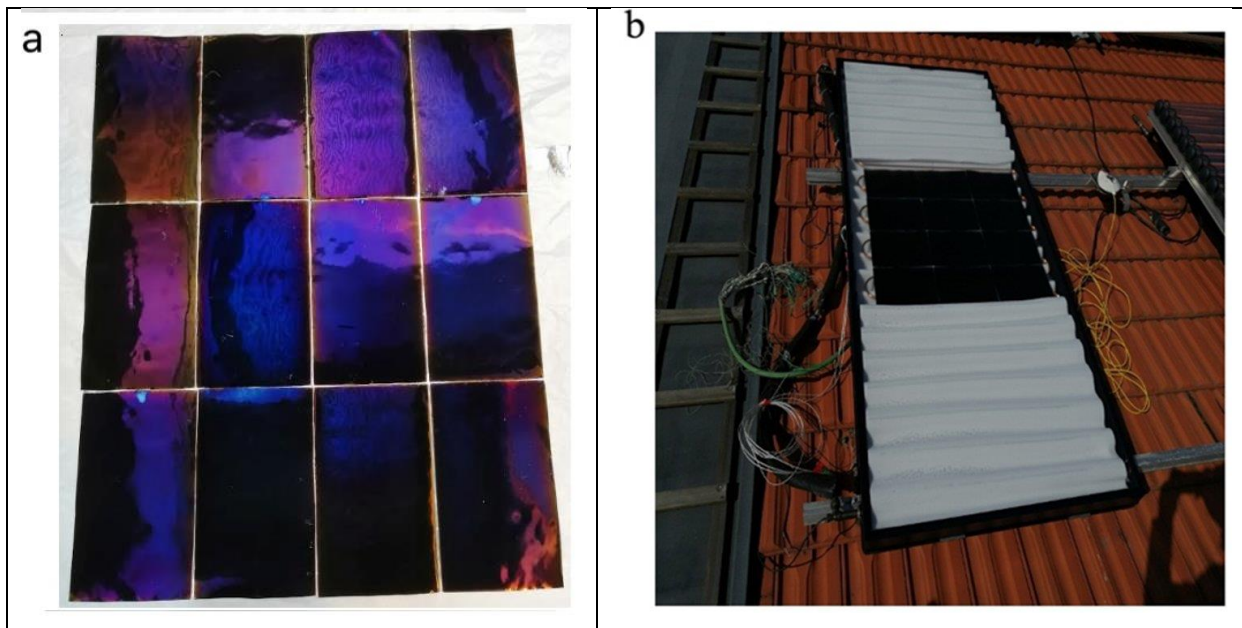


Fig. 10. a – View of 12 elemental mode-prepared LaCoO₃ samples assembled with a post-annealing thickness of 600 nm (annealing for 10 minutes at 600 °C), **b** – instrumented prototype of solar collector.

The prototype was installed at a tilt angle of 45 ° in the test zone of the Viessmann factory in Faulquemont (France). The circulation pump of the coolant was shut down to simulate the stagnation conditions. Thus, the heat transport fluid was maintained still during the measurements of temperature evolution as a function of exposure time (Fig. 11).

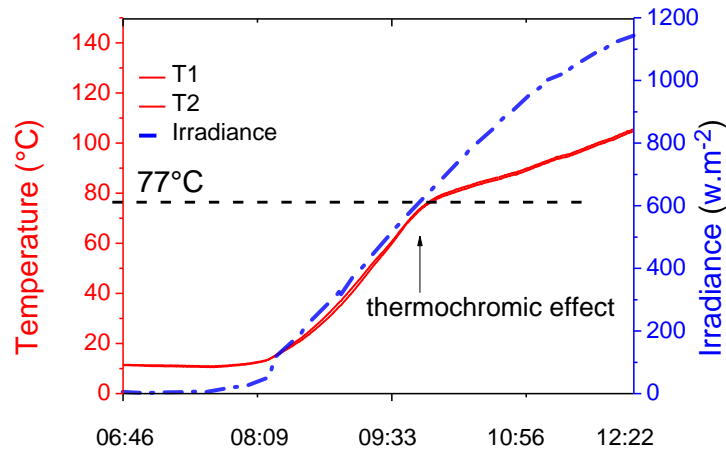


Fig. 11. Evolution of the temperature of prototype solar absorber as a function of exposure time.

The irradiance curve does not demonstrate any irregularities, meaning cloudless conditions beneficial for the measurements. When irradiance increase the temperature of the coolant increases, but the temperature curve shows a stall at around 77 °C attributed to the thermochromic effect that restrain limiting the increase of the temperature.

The complete evaluation of the emissivity changes with the temperature increment for a film used in the production of the prototype is presented in Fig. 12.

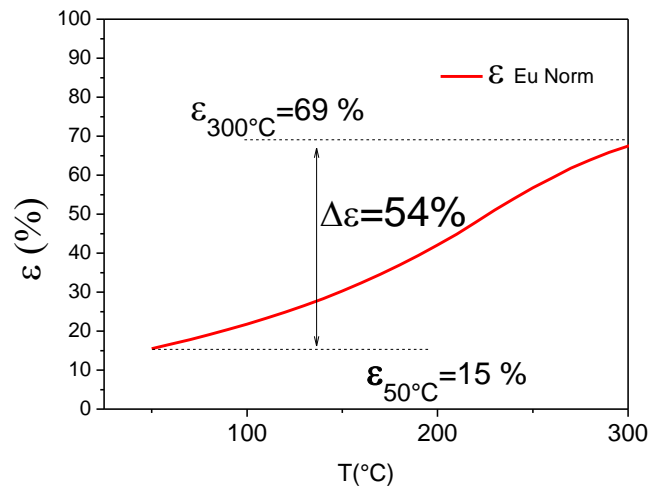


Fig. 12. Emissivity vs temperature for the prototype.

These results indicate that even though T_{MI} of $LaCoO_3$ is located around 220 °C, the transition starts at a far lower temperature and takes place over a much wider range than in the case of VO_2 . In fact, already between 40 and 80 °C the emissivity of our sensor shows an increase of the emissivity equal to 8.5%. That confirms the high potential of $LaCoO_3$ for the usage as a selective thermochromic layer for passive thermal regulation.

IV CONCLUSIONS

As-deposited elemental mode LaCoO_3 films present a multilayer structure that impedes the formation of the perovskite. To solve that problem, we deposit La and Co in the compound mode that allows thinner multilayers in the as-deposited thin films. Post-annealing SIMS measurements show that oxygen is present in the films regardless of the deposition mode with an equivalent oxygen profile. As expected, TEM measurements show a better homogeneity of the chemical elements and finally a better LaCoO_3 crystallinity. For the elemental mode prepared films, the elements are distributed in clearly discernible multilayers of approximately 10-12 nm, but TEM cross-sectional evaluations reveal that pre-oxidized films deposited in the compound mode possess *quasi*-homogeneous microstructure. In addition, the temperature of crystallization is lowered to 520 °C compared to 600 °C necessary in the case of the elemental mode. Differences observed in the XRD diagrams and the enhancement of the optical properties in the compound mode are attributed to the heterogeneity of the chemical composition. Concerning the optical properties and for 200 nm thick samples, selective layers elaborated in compound mode present a variation of the emissivity ($\Delta\epsilon$) that reaches 28% compare to the 16% obtained in the elemental mode. Considering this, the compound mode must be preferred but we also note in our previous studies that $\Delta\epsilon$ increases when the thickness increase. Unfortunately, the deposition rate of the compound mode synthesis (approx. 2 nm/min.) is far slower than the elemental deposition process and needs further optimization in order to be considered as an industrial technique for large-scale production. Therefore, it is industrially-preferable to opt for the rapid growth (42 min.) in the elemental deposition mode, as it allows the production of a film with a thickness of 600 nm that present a $\Delta\epsilon=54\%$ and a thermochromic effect starting at 77 °C.

In order to demonstrate the potentiality of the lanthanum cobaltite as selective layer avoiding overheating, we chose to build a prototype with annealed elemental mode prepared LaCoO_3 films of 600 nm thick which showed excellent thermal regulation performance with a thermochromic effect starting at 77 °C.

ACKNOWLEDGEMENTS

This work was financed by Viessmann Faulquemont SAS in the framework of the joint laboratory SOLARIS (Institut Jean Lamour – Nancy, France).

[1] P. Laffez, M. Zaghrioui, L. Reversat, P. Ruello, Electron doped $(\text{Sm}_{1-x}\text{Ca}_x)\text{MnO}_3$ perovskite manganite as potential infrared thermochromic switch, *Applied physics letters*, 8 (2006) 89. <https://doi.org/10.1063/1.2236290>

[2] G. Tang, Y. Yu, W. Chen, Y. Cao, Thermochromic properties of manganese oxides $\text{La}_{1-x}\text{A}_x\text{MnO}_3$ (A= Ca, Ba). *Materials Letters*, 62 (2008) 2914-2916. <https://doi.org/10.1016/j.matlet.2008.01.074>

[3] M. Soltani, M. Chaker, X. X. Jiang, D. Nikanpour, J. Margot, Thermochromic $\text{La}_{1-x}\text{Sr}_x\text{MnO}_3$ ($x= 0.1, 0.175, \text{ and } 0.3$) smart coatings grown by reactive pulsed laser deposition, *Journal of Vacuum Science & Technology*, 24 (2006) 1518-1523. <https://doi.org/10.1116/1.2204923>

[4] C. Wu, J. Qiu, J. Wang, M. Xu, L. Wang, Thermochromic property of $\text{La}_{0.8}\text{Sr}_{0.2}\text{MnO}_3$ thin-film material sputtered on quartz glass. *Journal of Alloys and Compounds*, 2 (2010) 506. <https://doi.org/10.1016/j.applthermaleng.2012.07.046>

[5] A. Boileau, F. Capon, S. Barrat, P. Laffez, J. F. Pierson, Thermochromic effect at room temperature of $\text{Sm}_{0.5}\text{Ca}_{0.5}\text{MnO}_3$ thin films. *Journal of Applied Physics*, 11 (2012) 111. <https://doi.org/10.1063/1.4722264>

[6] D. Vernardou, M.E. Pemble, D.W. Sheel. In-situ Fourier transform infrared spectroscopy gas phase studies of vanadium (IV) oxide coating by atmospheric pressure chemical vapor deposition using vanadyl (IV) acetylacetonate, *Thin Solid Films*, 14 (2008) 4502-4507. <https://doi.org/10.1016/j.tsf.2007.06.026>

- [7] D. Louloudakis, D. Vernardou, E. Spanakis, M. Suche, G. Kenanakis, M. Pemble, K. Savvakis, N. Katsarakis, E. Koudoumas, G. Kiriakidis, Atmospheric pressure chemical vapor deposition of amorphous tungsten doped vanadium dioxide for smart window applications, *Advanced Materials Letters*, 7 (2016) 192-196. <https://doi.org/10.5185/amlett.2016.6024>
- [8] S. Föste, A. Pazidis, R. Reineke-Koch, B. Hafner, D. Mercs, C. Delord, Flat plate collectors with thermochromic absorber coatings to reduce loads during stagnation, *Energy Procedia*, 91 (2016) 42-48. <https://doi.org/10.1016/j.egypro.2016.06.169>
- [9] D. Mercs, F. Capon, A. Corvisier, Matériau absorbant et panneau solaire utilisant un tel matériau (2014) WO2014140499A1.
- [10] D. Mercs, A. Didelot, F. Capon, J.F. Pierson, B. Hafner, A. Pazidis, R. Reineke-Koch, Innovative smart selective coating to avoid overheating in highly efficient thermal solar collectors, *Energy Procedia*, 91 (2016) 84-93. <https://doi.org/10.1016/j.egypro.2016.06.177>
- [11] B. Epp, Solar Keymark: Additional Table Allows Comparison of Annual Collector Output (2012).
- [12] R. H. Potze, G. A. Sawatzky, M. Abbate, Possibility for an intermediate-spin ground state in the charge-transfer material SrCoO₃, *Physical Review B*, 51 (1995) 11501. <https://doi.org/10.1103/PhysRevB.51.11501>
- [13] C. Zobel, M. Kriener, D. Bruns, J. Baier, M. Grüninger, T. Lorenz, A. Revcolevschi, Evidence for a low-spin to intermediate-spin state transition in LaCoO₃, *Physical Review B*, 66 (2002) 020402. <https://doi.org/10.1103/PhysRevB.66.020402>
- [14] H. Seim, M. Nieminen, L. Niinistö, H. Fjellvåg, L. S. Johansson, Growth of LaCoO₃ thin films from β-diketonate precursors. *Applied Surface Science*, 112 (1997) 243-250. [https://doi.org/10.1016/S0169-4332\(96\)01001-X](https://doi.org/10.1016/S0169-4332(96)01001-X)
- [15] H. J. Hwang, M. Awano, Preparation of LaCoO₃ catalytic thin film by the sol-gel process and its NO decomposition characteristics. *Journal of the European Ceramic Society*, 21 (2001) 2103-2107. [https://doi.org/10.1016/S0955-2219\(01\)00181-9](https://doi.org/10.1016/S0955-2219(01)00181-9)
- [16] M. Losurdo, A. Sacchetti, P. Capezzuto, G. Bruno, L. Armelao, D. Barreca, E. Tondello, Optical and electrical properties of nanostructured LaCoO₃ thin films, *Applied Physics Letters*, 87 (2005) 061909. <https://doi.org/10.1063/1.2009057>
- [17] D. N. Kharkhan, D. Pilloud, S. Bruyère, S. Migot, S. Barrat, F. Capon, Influence of as-deposited non-uniform stoichiometry on thermochromic properties of LaCoO₃ selective layers. *Journal of Applied Physics*, 127 (2020) 015304. <https://doi.org/10.1063/1.512514>
- [18] M. Palcut, K. Wiik, T. Grande, Cation self-diffusion in LaCoO₃ and La₂CoO₄ studied by diffusion couple experiments. *The Journal of Physical Chemistry B*, 111 (2007) 2299-2308. <https://doi.org/10.1021/jp068343s>
- [19] M. Palcut, J. S. Christensen, K. Wiik, T. Grande, Impurity diffusion of Pr in LaMnO₃, LaCoO₃ and LaFeO₃ materials. *Physical Chemistry Chemical Physics*, 10 (2008) 6544. <https://doi.org/10.1039/B808789J>
- [20] J. Philibert, Diffusion et transport de matière dans les solides, les Éditions de Physique, (1985).
- [21] M. E. Glicksman, Diffusion in solids: field theory, solid-state principles, and applications. New York, (2000), 54-56.
- [22] M. C. Benoudia, Interdiffusion et déformations dans des multicouches Cu/Ni et Mo/V: Diffraction des rayons X et simulation de la cinétique (Doctoral dissertation), (2009).
- [23] I. Safi, Recent aspects concerning DC reactive magnetron sputtering of thin films: a review. *Surface and Coatings Technology*, 127 (2000) 203-218. [https://doi.org/10.1016/S0257-8972\(00\)00566-1](https://doi.org/10.1016/S0257-8972(00)00566-1)
- [24] M. Benkahoul, M. Chaker, J. Margot, E. Haddad, R. Krizelecky, B. Wong, Thermochromic VO₂ film deposited on Al with tunable thermal emissivity for space applications. *Solar Energy Mater Sol Cells*, 95 (2011) 3504. <https://doi.org/10.1016/j.solmat.2011.08.014>